Aalborg Universitet

AALBORG UNIVERSITY
DENMARK

An Analysis of Modified Demodulation-Based Grid Voltage Parameter Estimator

Golestan, Saeed ; Guerrero, Josep M.

An Analysis of Modified Demodulation Based Grid Voltage Parameters Estimator

Saeed Golestan, *Senior Member, IEEE* and Josep M. Guerrero, *Fellow, IEEE*

Abstract—The estimation of the grid voltage fundamental parameters, i.e., the phase, frequency and amplitude, is required for a wide variety of applications, particularly for synchronization and control of grid-connected converters and for monitoring and protection purposes in power systems. To accomplish this task, many approaches have been proposed in literature. Recently, a modified demodulation based technique (MDT) has been presented, which aims to accurately extract the grid voltage fundamental parameters under harmonically distorted and frequency-varying conditions. In this letter, it is shown that the MDT is actually a phase-locked loop. The MDT small-signal modeling and stability analysis are then conducted, and some modifications to enhance its performance are suggested. The effectiveness of these modifications is finally confirmed using numerical results.

Index Terms—Demodulation technique, frequency measurement, fundamental frequency, phase detection, phase-locked loop (PLL), synchronization.

I. INTRODUCTION

The accurate extraction of the grid voltage fundamental parameters, i.e., the phase, frequency and amplitude, is essential in a wide variety of applications, such as interconnecting distributed generation systems to the grid, islanding detection of microgrids, control of grid-connected power converters and monitoring and protection of power systems [1]-[3].

Different approaches have been proposed in the literature to estimate the fundamental parameters of the grid voltage. The zero-crossing detection (ZCD) based method is probably the simplest one. The ZCD approach, however, suffers from a poor performance under noisy and harmonically distorted conditions [4]. To overcome this drawback, some approaches have been proposed in [5], [6].

The methods based on phase-locked loops (PLLs) are popular because they are often easy to implement digitally and offer a robust performance. These approaches can generally be understood as a standard PLL with a filtering stage, which is used to improve the PLL speed/accuracy trade-off. Indeed, the main difference among the PLL based techniques often lies in the type and location of the filtering technique they use in their structure. The moving average filter (MAF) [7], the notch filter [8], the repetitive regulator [9], the *dq*-frame cascaded delayed signal cancellation operator [10]-[12] and the conventional low-pass filters (LPFs) [13] are popular in-loop filtering stages, and the $\alpha\beta$-frame cascaded delayed signal

cancellation [10], [11], [14] and the complex coefficient filters [15] are well-known prefiltering stages.

The discrete Fourier transform (DFT) based approaches are also widely used in practice for the estimation of grid voltage parameters. The implementation of these techniques, however, demands a high computational effort. The DFT computational burden, of course, can be reduced by using a recursive implementation [16]. The recursive DFT, however, suffers from some stability issues, which demands some modifications to avoid them [17].

A modified demodulation based technique (MDT) has recently been presented in [18], which aims to deal with the shortcomings of available approaches and provide an accurate estimation of the grid voltage fundamental parameters in single-phase applications. The objective of this letter is to provide a detailed analysis of this technique. The small-signal modeling and stability analysis of this technique are also carried out and some modifications to enhance its performance are proposed.

II. OVERVIEW AND ANALYSIS OF CONVENTIONAL AND MODIFIED DEMODULATION TECHNIQUES

Fig. 1 shows the schematic of the conventional demodulation technique (CDT) for the grid voltage amplitude and frequency estimation in single-phase systems. In this technique, the single-phase system is considered as an unbalanced two-phase system, in which the first phase (α-axis voltage component) is the single-phase voltage signal and the second phase (β-axis voltage component) is zero. The $\alpha\beta$ voltage components are then transformed to the synchronous (dq) reference frame rotating by applying the Park's transformation with a rotating angle $\theta_n = \int \omega_n dt$, where ω_n is the nominal value of the grid frequency. Assuming the single-phase grid voltage is as

$$v(t) = V \cos(\theta) \tag{1}$$

where V and $\theta = \int \omega dt$ are the amplitude and phase-angle of the gird voltage, respectively, and ω is the grid frequency, the dq-axis voltage components can be obtained as

$$\begin{bmatrix} v_d(t) \\ v_q(t) \end{bmatrix} = \begin{bmatrix} \cos(\theta_n) & \sin(\theta_n) \\ -\sin(\theta_n) & \cos(\theta_n) \end{bmatrix} \begin{bmatrix} v(t) \\ 0 \end{bmatrix}$$

$$= \begin{bmatrix} \frac{V}{2}\cos(\theta - \theta_n) + \frac{V}{2}\cos(\theta + \theta_n) \\ \frac{V}{2}\sin(\theta - \theta_n) - \frac{V}{2}\sin(\theta + \theta_n) \end{bmatrix}. \tag{2}$$

As (2) shows, v_d and v_q both are consisted of a (near) dc term and a (near) double frequency term. To attenuate these double frequency terms, v_d and v_q are passed through two

S. Golestan and J. M. Guerrero are with the Department of Energy Technology, Aalborg University, Aalborg DK-9220, Denmark (e-mail: s.golestan@ieee.org; joz@et.aau.dk).
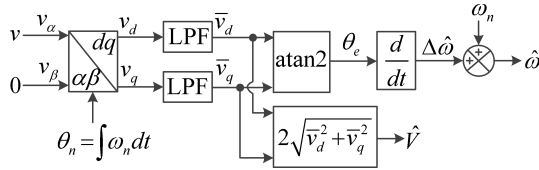
Fig. 1. Schematic of the CDT.

LPFs. Assuming these LPFs are ideal, their outputs in steady-state can be expressed as

$$\bar{v}_d(t) = \frac{V}{2} \cos\left(\theta - \theta_n + \varphi_{\text{LPF}}\right) \tag{3}$$

$$\bar{v}_q(t) = \frac{V}{2} \sin\left(\theta - \theta_n + \varphi_{\text{LPF}}\right) \tag{4}$$

where φ_{LPF} is the phase shift caused by the LPF under off-nominal grid frequencies. Applying the inverse tangent function to the LPFs output signals gives the phase error signal $\theta_e = \theta - \theta_n + \varphi_{\text{LPF}}$. The grid voltage frequency is then obtained by differentiating from θ_e and adding ω_n to the result. The grid voltage amplitude, on the other hand, can be calculated as 2 times the square root of the sum of the squares of the LPFs output signals.

The main drawback of the CDT is that the estimated qualities by this technique suffer from a considerable double-frequency oscillatory error, because the LPFs are not able to completely block the double frequency terms of v_d and v_q. To deal with this drawback, the MDT is proposed in [18]. Fig. 2 shows the schematic of this technique, in which a double frequency cancelation (DFC) unit to reject the double frequency terms of v_d and v_q is used. It should be mentioned that the DFC unit in this technique is almost the same as the double frequency and amplitude compensation (DFAC) structure proposed in [19]. The operating principle of the DFC unit and MDT is briefly explained in what follows.

In the MDT, the $\alpha\beta$-axis voltages are transferred to a synchronous reference frame rotating at the same angular frequency as the grid voltage angular frequency. Therefore, the dq-axis voltages in this technique can be expressed as

$$v_d(t) = \frac{V}{2} \cos\overbrace{\left(\theta - \hat{\theta}\right)}^{\theta_e} + \frac{V}{2} \cos\left(\theta + \hat{\theta}\right) \tag{5}$$

$$v_q(t) = \frac{V}{2} \sin\left(\theta - \hat{\theta}\right) - \frac{V}{2} \sin\left(\theta + \hat{\theta}\right) \tag{6}$$

or equivalently

$$v_d(t) = \frac{V}{2} \cos\left(\theta_e\right) + \frac{V}{2} \cos\left(\theta_e\right)\cos\left(2\hat{\theta}\right) - \frac{V}{2} \sin\left(\theta_e\right)\sin\left(2\hat{\theta}\right) \tag{7}$$

$$v_q(t) = \frac{V}{2} \sin\left(\theta_e\right) - \frac{V}{2} \sin\left(\theta_e\right)\cos\left(2\hat{\theta}\right) - \frac{V}{2} \cos\left(\theta_e\right)\sin\left(2\hat{\theta}\right). \tag{8}$$

As (7) and (8) show, v_d and v_q both are consisted of a dc term and two double frequency terms. Notice that the amplitudes of these double frequency terms are the same as dc terms of v_d and v_q and that the LPFs output signals, i.e., $\bar{v}_d$ and $\bar{v}_q$, provide an estimation of these dc terms. Therefore, the double frequency terms of v_d and v_q can be easily cancelled out by
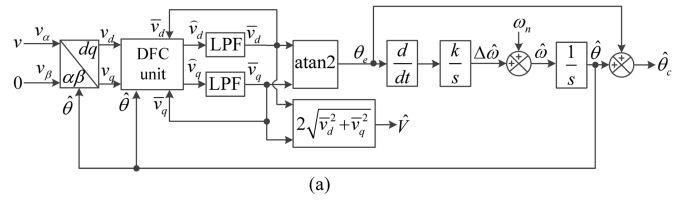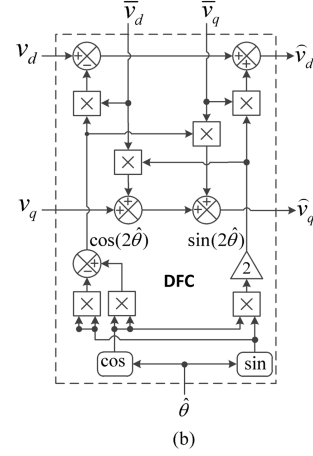
Fig. 2. (a) Schematic of the MDT. (b) DFC unit.

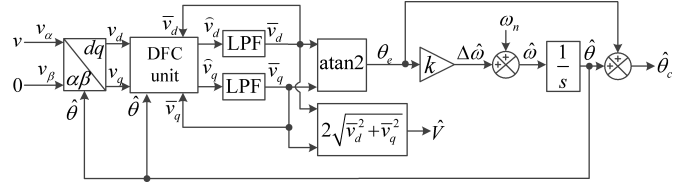Fig. 3. Alternative mathematically equivalent representation of the MDT.

reconstructing and subtracting them from v_d and v_q, as shown in Fig. 2(b). A more detailed description of the DFC unit can be found in [19].

After cancelling the double frequency terms of v_d and v_q and extracting their dc terms, the amplitude normalization task is carried out by calculating $\text{atan2}(\bar{v}_q, \bar{v}_d)$. Using the arctangent function in the amplitude normalization is also useful to remove (or at least to reduce) the nonlinearity of the control loop [20], [21]. The steady-state output of the arctangent function is the phase error signal $\theta_e = \theta - \hat{\theta}$, which is differentiated and subsequently passed through an integrator with gain k. The developers of the MDT [18], however, do not explain why they have do that. Indeed, cascading a differentiator and an integrator with gain k is mathematically equivalent with a simple gain k. Considering this fact, the alternative mathematically equivalent representation of the MDT can be obtained as shown in Fig. 3. A comparison of this structure with the quasi-type-1 PLL (QT1-PLL) [20], shown in Fig. 4, clearly indicates that the MDT is actually the single-phase version of the QT1-PLL, but with a DFC unit. Therefore, to better understand the MDT performance, the QT1-PLL operating principle is explained in the following. Before that, a general background on developing the QT1-PLL is presented.

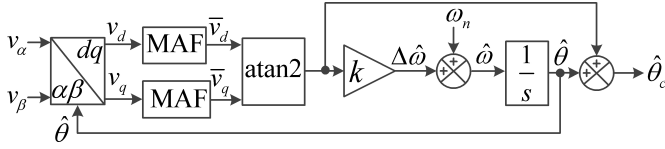Conventional PLLs typically employ a proportional-integral
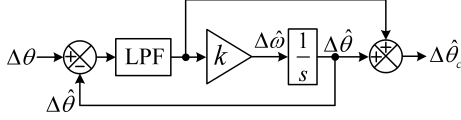
Fig. 4. Schematic of the QT1-PLL [20].

Fig. 5. Small-signal model of the MDT.

Fig. 6. Accuracy assessment of the MDT small-signal model.

Fig. 7. Open-loop Bode plot of the MDT with the same parameters designed in [18].

(PI) controller as their loop filter (LF). This structure, however, has a limited filtering capability. To further improve the PLL filtering ability, an additional LPF (e.g., a MAF) can be incorporated into the control loop. This additional LPF, however, increases the phase delay in the PLL control loop and, therefore, slows down its dynamic response. To deal with this problem, the QT1-PLL structure is suggested in [20]. In the QT1-PLL, the PI controller is replaced with a simple gain, which reduces the phase delay in the PLL control-loop, but makes the PLL a type-1 control system. This means that the PLL cannot track frequency drifts with a zero phase-error. To solve this issue, the arctangent output signal is added to the PLL output. This act provides an additional open-loop pole at the origin and, therefore, enables the PLL to achieve a zero phase error in the presence of frequency drifts [20].

III. SMALL-SIGNAL MODELING AND STABILITY ANALYSIS

As shown in the previous Section, the MDT can be understood as the single-phase version of the QT1-PLL, but with the DFC unit. On the other hand, the DFC unit, which acts like a notch filter with notch frequency at twice the grid fundamental frequency, has a negligible effect on the MDT dynamics and stability on the condition that the MDT closed-loop bandwidth is sufficiently smaller than 2ω. Considering these facts, the same small-signal model as the QT1-PLL model can be considered for the MDT. The QT1-PLL small-signal model has already been derived in [20]. Fig. 5 shows the MDT small-signal model, in which Δ denotes perturbations around the nominal operation point.

To evaluate the accuracy of the derived model, a performance comparison between the MDT and the model under a phase-angle jump of $+40$ and a frequency step change of $+2$ Hz is carried out. In this evaluation, the same parameters as those designed in [18], i.e., a third-order LPF with cutoff frequency of $\omega_n/3$ and $k = 25$, are considered. Fig. 6 shows the obtained results. As it can be observed, the derived model accurately predicts the MDT dynamic behavior.

Fig. 7 illustrates the open-loop Bode plot of the MDT using the same parameters designed in [18]. Notice that the open-loop transfer function can simply be obtained by rearranging the MDT small-signal model to its equivalent classical feedback form, as shown in Fig. 8. Anyway, as it can be observed
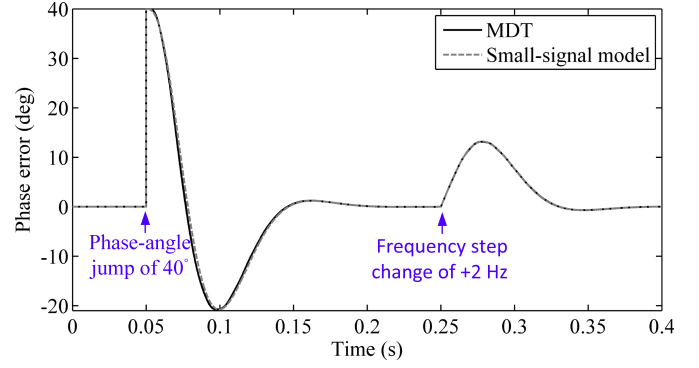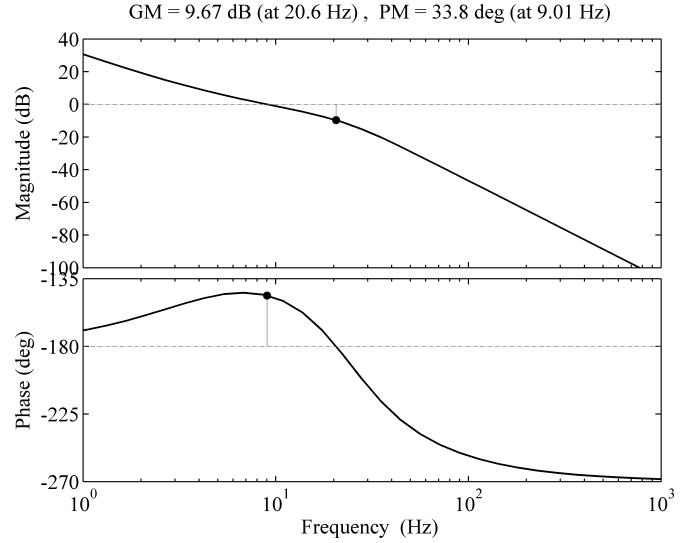
in Fig. 7, the crossover frequency is rather low, which implies the MDT suffers from a rather slow dynamic response. This fact was already confirmed in the accuracy assessment of the small-signal model. The stability margins of the MDT are acceptable, but a higher phase margin (PM) to reduce the phase overshoot during phase-angle jumps is favourable. The MDT phase overshoot when using the parameters designed in [18] is around 50%.

IV. MDT PERFORMANCE ENHANCEMENT

Improving the MDT dynamic performance and stability margin while maintaining a good harmonic filtering capability for that is the aim of this section. To accomplish this objective, using two cascaded MAFs instead of the third-order LPF in
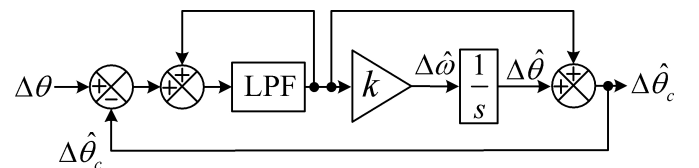

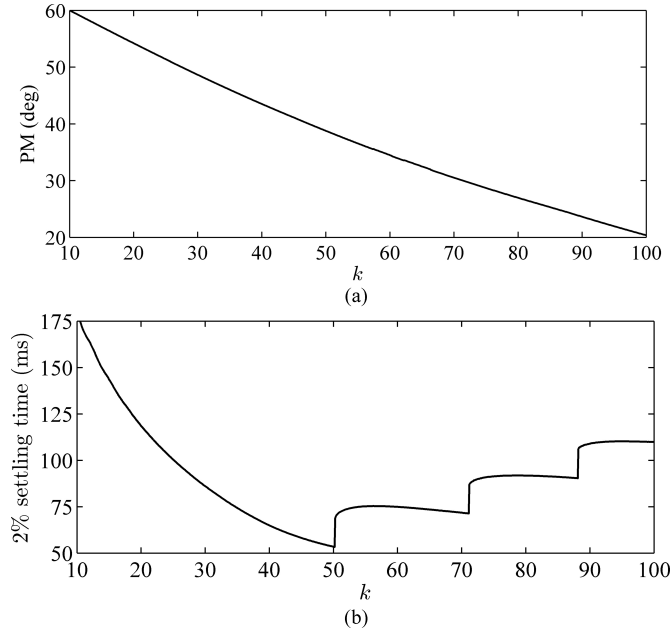Fig. 8. Classic feedback form of the model shown in Fig. 5.

Fig. 9. (a) PM and (b) 2% settling time of the MDT as a function of k.

the MDT structure is suggested in this letter. The s-domain transfer function of the MAF is

$$G_{\mathrm{MAF}}(\mathrm{s}) = \frac{1 - e^{-T_w s}}{T_w s} \qquad (9)$$

where T_w is its window length.

There are two typical choices for the MAF window length: 1) $T_w = T/2$ (T is the grid fundamental period) that enables the MDT to block the odd-order harmonics of the grid voltage, which appear as even-order harmonics in its control loop; and 2) $T_w = T$ that enables the MDT to block both even-order and odd-order harmonics of the grid voltage [22]. Considering that the even-order harmonics of the grid voltage are often small and $T_w = T$ significantly increases the phase delay in the MDT control loop, $T_w = T/2$ is selected in this letter.

Equations (10) and (11) describes the open-loop and closed-loop transfer functions of the MDT when using two cascaded MAFs as the LPF

$$G_{ol}(s) = G_{\mathrm{MAF}}^2(s) \frac{s + k}{s\left(1 - G_{\mathrm{MAF}}^2(s)\right)} \qquad (10)$$

$$G_{cl}(s) = G_{\mathrm{MAF}}^2(s) \frac{s + k}{s + k G_{\mathrm{MAF}}^2(s)}. \qquad (11)$$

Using these transfer functions, the variations of the MDT PM and 2% settling time (in response to a phase-angle jump) as a function of k can be obtained as shown in Fig. 9. As it can be observed, minimizing the settling time requires selecting a value around 50 for k. $k = 48$ is chosen in this letter, which provides a PM around 40°, a 2% settling time around 2.5 cycles of the nominal frequency, and a phase overshoot around 37%.

V. NUMERICAL RESULTS

In this section, a performance comparison between the MDT structure proposed in [18] (hereafter called MDT1) and the
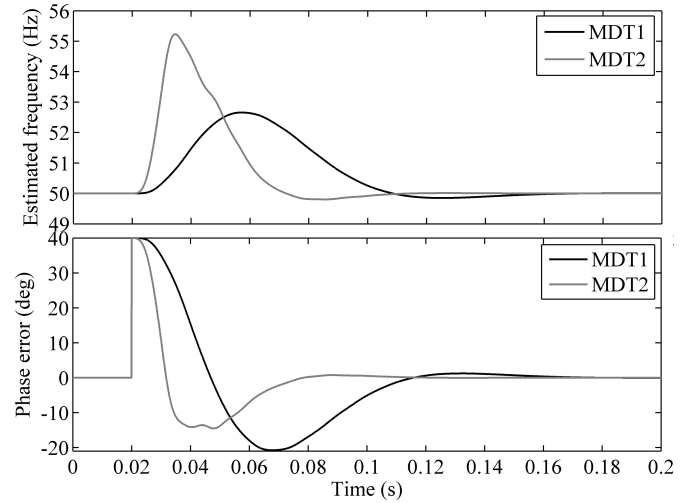
one proposed in this letter (from now on called MDT2) is carried out. Notice that the MDT2 has the same structure as that shown in Fig. 3, but the LPF block in that is replaced with two-cascaded MAFs with window length $T_w = T/2 = 0.01$ s. The gain k in the MDT1 and MDT2 is 25 and 48, respectively.

Five test cases are designed:

- Test case 1: The grid voltage undergoes a +40° phase-angle jump.
- Test case 2: The grid voltage experiences a +2 Hz frequency step change.
- Test case 3: The grid voltage is harmonically distorted. The total harmonic distortion (THD) of the grid voltage is 10.67% in this test.
- Test case 4: The grid voltage undergoes a 0.5 pu voltage sag.
- Test case 5: The grid voltage experiences a +10 Hz/s frequency ramping change.

Fig. 10 and 11 show the simulation results under the test cases 1 and 2, respectively. As it can be observed, the MDT2 provides a much faster dynamic response than the MDT1: The MDT2 2% settling time, which is around 2.5 cycles of the nominal frequency, is almost half of that of the MDT1. The MDT2 also offers a rather considerable decrease in the phase overshot and peak phase error under the test cases 1 and 2, respectively. The estimated frequency by the MDT2, however, experiences a larger transient under the test case 1. The reason is that the MDT2 has a higher bandwidth than MDT1, which results in an increased coupling between its phase and frequency variables. This issue has been discussed in detail in [23].

Fig. 12 illustrates the simulation results under the test case 3. As shown, the MDT2 provides a higher filtering capability than the MDT1 when the grid frequency is close to its nominal value, however its performance tends to worsen in the presence of large frequency drifts. According to the European standard EN50160, the grid frequency should be within the range of 50 ± 0.5 Hz in 99.5% of a week. Considering this fact, it can be concluded that the MDT2 is a better option from the
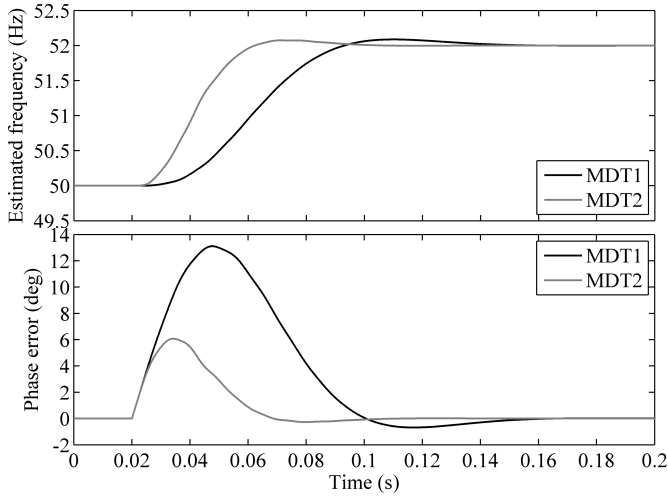

Fig. 10. Simulation results under the test case 1.

Fig. 11. Simulation results under the test case 2.

Fig. 12. Simulation results under the test case 3.

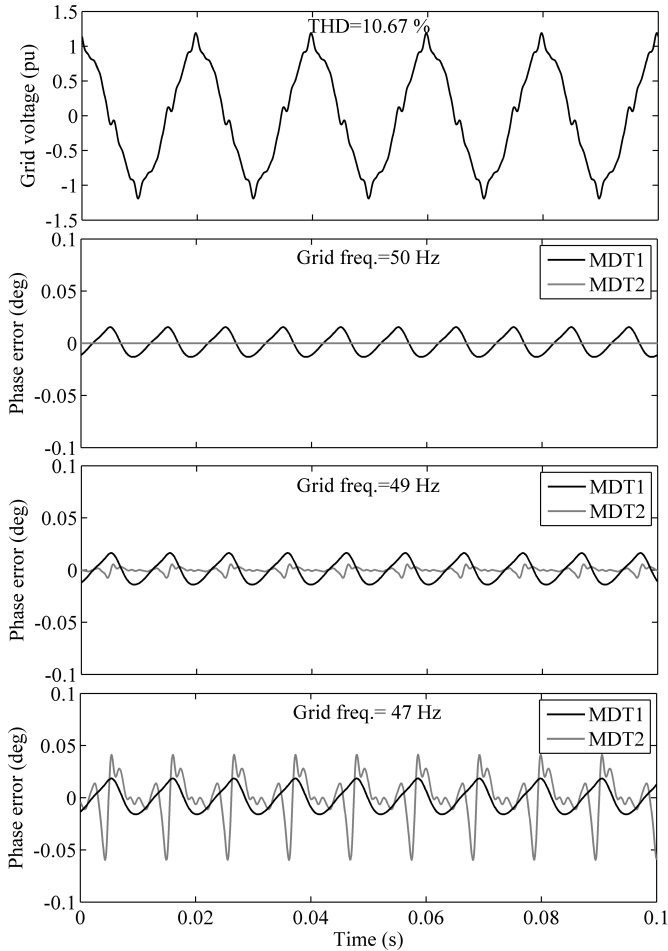Fig. 13. Simulation results under the test case 4.
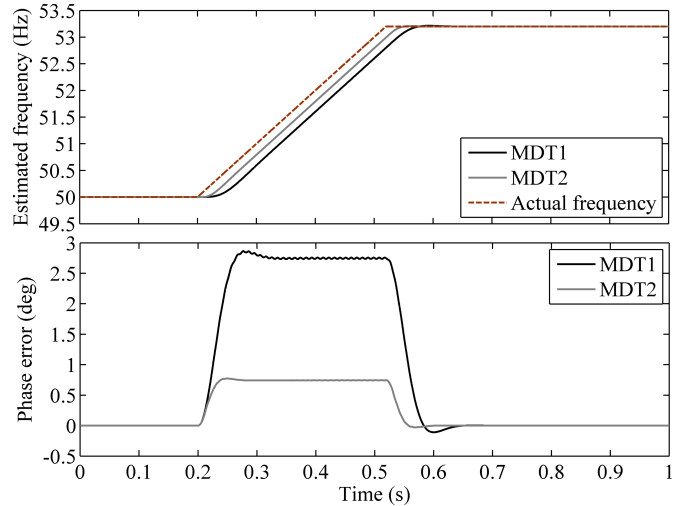
Fig. 14. Simulation results under the test case 5.

harmonic filtering point of view.

Simulation results under the test cases 4 and 5 can be observed in Fig. 13 and 14, respectively. Again, it can be observed that the MDT2 provides a much faster dynamic response. Providing a considerably lower phase error by the MDT2 during the frequency ramping interval is also notice-
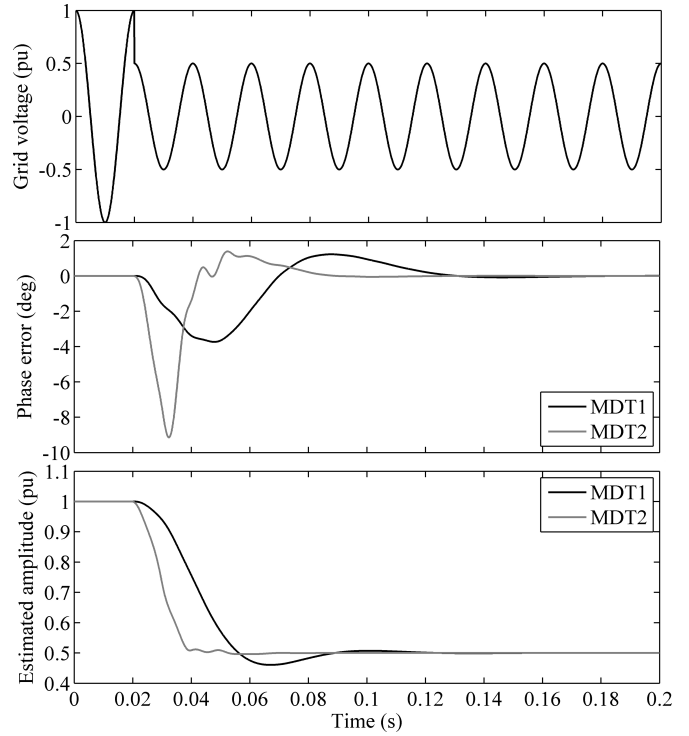
able.

VI. CONLCUSION

In this letter, an analysis of the MDT was carried out. It was shown that the MDT is a single-phase version of the QT1-PLL, but with a DFC unit. It was also shown that the same small-signal model as the QT1-PLL model can be considered for the stability analysis and dynamic performance evaluation of the MDT. Some modifications to enhance the stability margin and dynamic performance of the MDT was then proposed. The effectiveness of these modifications was verified using numerical results.

REFERENCES

[1] T. V. Tran, T. W. Chun, H. H. Lee, H. G. Kim, and E. C. Nho, "PLL-based seamless transfer control between grid-connected and islanding modes in grid-connected inverters," *IEEE Trans. Power Electron.*, vol. 29, no. 10, pp. 5218-5228, Oct. 2014.

[2] D. Dong, B. Wen, P. Mattavelli, D. Boroyevich, and Y. Xue, "Modeling and design of islanding detection using phase-locked loops in three-phase grid-interface power converters," *IEEE J. Emerg. Sel. Topics Power Electron.*, vol. 2, no. 4, pp. 1032-1040 , Dec. 2014.

[3] P. Roncero-Sanchez, X. del Toro Garcia, A. P. Torres, and V. Feliu, "Robust frequency-estimation method for distorted and imbalanced three-phase systems using discrete filters," *IEEE Trans. Power Electron.*, vol. 26, no. 4, pp. 1089-1101, Apr. 2011.

[4] M. Ciobotaru, *Reliable grid condition detection and control of single phase distributed power generation systems*, PhD Thesis. Aalborg University, 2009.

[5] H. Geng, D. Xu, and B. Wu, "A novel hardware-based all-digital phase-locked loop applied to grid-connected power converters," *IEEE Trans. Ind. Electron.*, vol. 58, no. 5, pp. 1737-1745, May 2011.

[6] B. Liu, F. Zhou, Y. Zhu, H. Yi, and F. Wang, "A three-phase PLL algorithm based on signal reforming under distorted grid conditions," *IEEE Trans. Power Electron.*, vol. 30, no. 9, pp. 5272-5283, Sep. 2015.

[7] L. Wang, Q. Jiang, L. Hong, C. Zhang, and Y. Wei, "A novel phase-locked loop based on frequency detector and initial phase angle detector," *IEEE Trans. Power Electron.*, vol. 28, no. 10, pp. 4538-4549, Oct. 2013.

[8] F. G. Espin, E. Figueres, and G. Garcera, "An adaptive synchronous reference-frame phase-locked loop for power quality improvement in a polluted utility grid," *IEEE Trans. Ind. Electron.*, vol. 59, no. 6, pp. 2718-2731, Jun. 2012.

[9] M. Rashed, C. Klumpner, and G. Asher, "Repetitive and resonant control for a single-phase grid-connected hybrid cascaded multilevel converter," *IEEE Trans. Power Electron.*, vol. 28, no. 5, pp. 2224-2234, May 2013.

[10] Y. F. Wang, and Y. Li, "Grid synchronization PLL based on cascaded delayed signal cancellation," *IEEE Trans. Power Electron.*, vol. 26, no. 7, pp. 1987-1997, Jul. 2011.

[11] Y. F. Wang, and Y. W. Li, "Analysis and digital implementation of cascaded delayed-signal-cancellation PLL," *IEEE Trans. Power Electron.*, vol. 26, no. 4, pp. 1067-1080, Apr. 2011.

[12] S. Golestan, M. Ramezani, J. M. Guerrero, and M. Monfared, "*dq*-frame cascaded delayed signal cancellation-based PLL: Analysis, design, and comparison with moving average filter-based PLL," *IEEE Trans. Power Electron.*, vol. 30, no. 3, pp. 1618-1632, Mar. 2015.

[13] S. Golestan, F.D. Freijedo, and J. M. Guerrero, "A systematic approach to design high-order phase-locked loops," *IEEE Trans. Power Electron.*, vol. 30, no. 6, pp. 2885-2890, Jun. 2015.

[14] S. Golestan, F. D. Freijedo, A. Vidal, A. G. Yepes, J. M. Guerrero, and J. Doval-Gandoy, "An efficient implementation of generalized delayed signal cancellation PLL," *IEEE Trans. Power Electron.*, vol. PP, no. 99, pp. 1-10, Apr. 2015.

[15] X. Guo, W. Wu, and Z. Chen, "Multiple-complex coefficient-filter based phase-locked loop and synchronization technique for three phase grid interfaced converters in distributed utility networks," *IEEE Trans. Ind. Electron.*, vol. 58, no. 4, pp. 11941204, Apr. 2011.

[16] B. P. McGrath, D. G. Holmes, and J. J. H. Galloway, "Power converter line synchronization using a discrete Fourier transform (DFT) based on a variable sample rate," *IEEE Trans. Power Electron.*, vol. 20, no. 4, pp. 877-884, July 2005.

[17] H. A. Darwish and M. Fikri, "Practical considerations for recursive DFT implementation in numerical relays," *IEEE Trans. Power Del.*, vol. 22, no. 1, pp. 42-49, Jan. 2007.

[18] Md. S. Reza, M. Ciobotaru, and V. G. Agelidis, "A modified demodulation technique for single-phase grid voltage fundamental parameters estimation," *IEEE Trans. Ind. Electron.* vol. 62, no. 6, pp. 3705-3713, Jun. 2015.

[19] S. Golestan, M. Monfared, F. D. Freijedo, and J. M. Guerrero, "Design and tuning of a modified power-based PLL for single-phase grid connected power conditioning systems," *IEEE Trans. Power Electron.*, vol. 27, no. 8, pp. 3639-3650, Aug. 2012.

[20] S. Golestan, F. D. Freijedo, and A. Vidal, J. M. Guerrero, and J. D. Gandoy, "A quasi-type-1 phase-locked loop structure," *IEEE Trans. Power Electron.*, vol. 29, no. 12, pp. 6264-6270, Dec. 2014.

[21] I. Serban and C. Marinescu, "Enhanced control strategy of three-phase battery energy storage systems for frequency support in microgrids and with uninterrupted supply of local loads," *IEEE Trans. Power Electron.*, vol. 29, no. 9, pp. 5010-5020, Sep. 2014.

[22] S. Golestan, M. Ramezani, J. M. Guerrero, F. D. Freijedo, and M. Monfared, "Moving Average Filter Based Phase-Locked Loops: Performance Analysis and Design Guidelines," *IEEE Trans. Power Electron.*, vol. 29, no. 6, pp. 2750-2763, Jun. 2014.

[23] M. Karimi-Ghartemani, S. A. Khajehoddin, P. K. Jain, and A. Bakhshai, "Problems of startup and phase jumps in PLL systems," *IEEE Trans. Power Electron.*, vol. 27, no. 4, pp. 1830-1838, Apr. 2012.